Carbohydrate Polymers 155 (2017) 192–200

Contents lists available at ScienceDirect

Carbohydrate Polymers

journal homepage: www.elsevier.com/locate/carbpol

Integration of lysozyme into chitosan nanoparticles for improving antibacterial activity

Tiantian Wu[a], Chunhua Wu[a,b], Shalu Fu[a], Liping Wang[a], Chunhong Yuan[c], Shiguo Chen[a], Yaqin Hu[a,*]

[a] Department of Food Science and Nutrition, Zhejiang Key Laboratory for Agro-Food Processing, Fuli Institute of Food Science, Zhejiang University, Zhejiang R & D Center for Food Technology and Equipment, Hangzhou 310058, PR China
[b] Division of Applied Biosciences, Graduate School of Agriculture, Kyoto University, Kyoto, Japan
[c] Department of Food Production and Environmental Management, Faculty of Agriculture, Iwate University, Morioka, Iwate 020-8550, Japan

ARTICLE INFO

Article history:
Received 14 May 2016
Received in revised form 19 August 2016
Accepted 25 August 2016
Available online 25 August 2016

Keywords:
Chitosan nanoparticles
Chitosan-lysozyme nanoparticles
Sodium tripolyphosphate
Ionotropic gelation
Antibacterial activity

ABSTRACT

Lysozyme was integrated into chitosan nanoparticles (CS-NPs) to improve the antibacterial activity. CS-NPs and chitosan-lysozyme nanoparticles (CS-Lys-NPs) were prepared according to the ionic gelation technique and then characterized by average size, zeta potential, polydispersity index (PDI), atomic force microscopy (AFM), fourier transform infrared (FT-IR), small-angle X-ray scattering (SAXS), circular dichroism (CD) and UV–visible spectroscopy. Antibacterial properties were investigated by transmission electron microscopy (TEM) based on observation of the inhibition zone and measurement of the minimum inhibitory concentration (MIC) and minimum bacterial concentration (MBC) of CS-NPs and CS-Lys-NPs against *E. coli and B. subtilis*. The CS-NPs had particle sizes of 476.2–548.1 nm, while an increase to ~488.8 to 613.5 nm was observed upon loading with lysozyme. The results suggested that the integration of lysozyme into CS-NPs enhanced the antibacterial activity against *E. coli* and *B. subtilis*, which may show great potential for use in the food industry and other applications in the form of direct addition or incorporation into packaging.

1. Introduction

Lysozyme is a small monomeric protein. It is a glycoside hydrolase composed of 129 amino acid residues, which contains four intact disulfide bonds, six tryptophan (Trp), three tyrosine (Tyr), three phenylalanine (Phe) residues (Jing, Chang et al., 2016; Jing, Song et al., 2016). lysozyme ubiquitously presents in various human tissues and secretions (Chen et al., 2005).The unique characteristic of anti-inflammatory, antiviral, antiseptic, antihistamine and antineoplastic activities make it has potential in pharmacological functions (Jash & Kumar, 2014). Lysozyme has been applied in the preservation of different food products (e.g. rawand processed meat, dairy products, fruits and vegetables) to extend the shelf life (Tiwari et al., 2009). Additionally, various applications of lysozyme were developed, such as the potential to be an antimicrobial agent in pharmaceuticals, home appliances and potential aseptic and therapeutic uses, which make lysozyme applications an interesting research area (Zheng, Wan, Yu, & Zhang, 2016).

It is well known that lysozyme can inhibit some gram positive bacteria for its unique ability to damage bacterial by hydrolyzing 1,4-β-linkage between N-acetyl- muramic acid and N-acetyl-D-glucosamine of bacterial cell wall peptidoglycan (Jollès, 1964; Yuan, Yin, Jiang, & Liang, 2013). However, gram negative bacteria are less sensitive toward lysozyme due to the presence of a protective lipopolysaccharide (LPS) on the bacterial cell wall. What is more, the practical application of free lysozyme is quite limited because this molecule is unstable and easily inactivated (Zhang et al., 2015).

To improve the quality of lysozyme, many methods were developed. Lysozyme combined with other antimicrobial agents exihibited a better antimicrobial activity (Chen et al., 2005). Besides, lysozyme was prepared in the forms of microcapsules, films, beads, nanoparticles etc. incorporated with other materials (Amara, Eghbal, Degraeve, & Gharsallaoui, 2016; Dekina, Romanovska, Ovsepyan, Tkach, & Muratov, 2016; Liburdi, Benucci, Palumbo, & Esti, 2015; Jing, Chang et al., 2016; Jing, Song et al., 2016). Wherein, protein/polysaccharide complexes are important for industrial applications. Sugars like sucrose can protect lysozyme structure by forming hydrogen bonds with protein molecules (Liao,

Abbreviations: CS, chitosan; CS, NPs chitosan nanoparticles; CS-Lys-NPs, chitosan-lysozyme nanoparticles; TPP, sodium tripolyphosphate.

* Corresponding author.
E-mail address: yqhu@zju.edu.cn (Y. Hu).

http://dx.doi.org/10.1016/j.carbpol.2016.08.076
0144-8617/

Brown, Nazir, Quader, & Martin, 2002).The coating of lysozyme with poly-γ-glutamic acid and chitosan can broaden the antibacterial spectrum of the composite lysozyme nano reagent, and improve antibacterial activity (Yong et al., 2013).

Chitosan (CS) is a positively charged polysaccharide formed by deacetylation of chitin. As the second most abundant biopolymer, chitin is ubiquitous in the cell wall of fungi and living organisms such as shrimps, crabs, insects and tortoises (Ravindra, Krovvidi, & Khan, 1998). CS can be used in solutions, hydrogels, micro-particles and nanoparticles because of its unique versatility. In addition, an endless array of CS derivatives can be prepared because of the existing amine, N-acetyl and hydroxyl groups. CS is widely used in the delivery system of proteins, drugs, vaccines and enzymes because of its excellent mucoadhesive characteristics, which extend the residual time at the absorption site (Sanyakamdhorn, Agudelo, & Tajmir-Riahi, 2013).

For a delivery system, it is vital to control characteristics such as particle size, particle distribution and surface charge because these parameters affect the behavior of core materials. There are significant connections between particle size and the effects on antigen delivery to antigen-presenting cells. It was reported that antigen-presenting cells such as dendritic cells (DC) could uptake particles of 0.5 μm and smaller with the best performance (Foged, Brodin, Frokjaer, & Sundblad, 2015). Lately, chitosan-based nanoparticles (CSNPs) have exhibited various advantages over the pattern chitosan. The enhanced antimicrobial activity and controlled release rate made chitosan-based nanoparticles an ideal candidate for applications in targeted delivery systems in the food and pharmacy industries. Compared to CS, the nano size and larger surface area contribute to the improved interactions between CSNPs and the microbial cell wall. The larger surface area allows nanoparticles to attach tightly onto the surface of bacteria, which damages the intracellular components and accelerates the death of cells, resulting in better antibacterial activities of CSNPs (Qi, Xu, Jiang, Hu, & Zou, 2004).

In the present study, CS nanoparticles were prepared, and lysozyme was integrated into CS-NPs based on the ionic gelation of chitosan with tripolyphosphate anions. Their antibacterial activities against gram negative bacteria *Escherichia coli* O_{157}:H_7 (ATCC25922) (*E. coli*) and gram positive bacteria *Bacillus subtilis* (ACCC10242) (*B. subtilis*) were examined. The morphological changes of *E. coli*/*B. subtilis* treated with CS, CS-NPs and CS-Lys-NPs were examined by transmission electron microscopy (TEM). And the secondary structure of lysozyme and its possibly interactions between chitosan particles were studied, which could contribute to the antimicrobial actions.

2. Materials and methods

2.1. Reagents and bacteria

Chitosan (molecular weight of 50,000 to 100,000) was purchased from Qingdao Yun Yu Biotechnology Co., Ltd. Lysozyme (from chicken egg white) and sodium tripolyphosphate (TPP) were purchased from Sigma Chemical Co. (St. Louis, MO, USA). Nutrient Broth (NB) and Nutrient Agar (NA) were purchased from Qingdao Hope Bio-Technology Co., Ltd. Acetic acid, sodium hydroxide, sodium dihydrogen phosphate, disodium hydrogen phosphate were of analytical grade (AR), and hydrochloric acid was of guarantee reagent (GR), all of these were purchased from Sinopharm Chemical Reagent Co., Ltd. *Bacillus subtilis* ACCC10242 (*B. subtilis*) was obtained from Life sciences insititute, Zhejiang university, China. *Escherichia coli* O_{157}:H_7 (ATCC25922) (*E.coli*) was purchased from China center of industrial culture collection (CICC).

2.2. Preparation of chitosan nanoparticles

Chitosan nanoparticles were prepared based on the ionotropic gelation between CS and sodium tripolyphosphate (TPP) as reported previously (Jang & Lee, 2008) with slight modifications. Briefly, solutions with CS-to-TPP ratios of 3:1 (V/V) were prepared and stirred at room temperature (25 ± 1 °C) to achieve complete dissolution, adjusting the final pH value to 4 and 5 with hydrochloric acid (1 M) and sodium hydroxide (1 M). CS-NPs were formed by the addition of 6 mL TPP (0.25%, W/V) solution using a peristaltic pump (BT100-2J, Hebei Lange current pump Ltd, China) to 18 mL CS solution (0.50%, W/V) under constant magnetic stirring for 1 h. Nanoparticles were purified by centrifugation at 10000 × *g* for 15 min. The precipitate was extensively rinsed with distilled water to remove unreacted substance and then freeze-dried with a freeze dryer (Labconco, Beijing Light Ace HK L-imited, China) for 2 days under −80 °C before further use or analysis.

Lysozyme was integrated into 10 mL CS nanoparticle suspensions (0.5% w/v) by adding lysozyme at five different concentrations, 0.25, 0.50, 0.75, 1.00 and 1.25 mg/mL, before purification. The purification was then carried out as described above for the CS-NPs. The pHs used were based on the antimicrobial actions according to previously studies (Hong, Na, Lee, & Meyers, 2002; Zhang et al., 2016) and preliminary analysis.

2.3. Characterization of CS-Lys-NPs

CS-NPs prepared at pH 5 and CS-Lys-NPs prepared at pH 5 with lysozyme concentrations of 1.25 mg/mL were characterized for most measurements based on the preliminary analysis of encapsulation efficiency, polydispersity index.

The particle size, polydispersity index (PDI) and zeta potential (ZP) of the resultant particles were determined by nano particle size and zeta potential analyzer (Zetasizer Nano ZS90, UK).

The surface micrographs were imaged by atomic force microscopy (AFM, Multimode, BRUKER Daltonics Inc., USA). CS, CS-NPs and CS-Lys-NPs solutions were added to the surface of a piece of mica plate (10 × 10 mm, Beijing Zhongjingkeyi Technology Co., Ltd, China) and dried naturally after 24 h before AFM observation.

Fourier transform infrared (FT-IR) spectroscopy (Thermo Scientific Nicolet Avatar 370, USA) was carried out to confirm information about chemical bonds or functional groups, with the spectrum collected from 4000 to 400 cm^{-1} at room temperature at 4 cm^{-1} resolution.

Diffraction patterns of small-angle X-ray scattering (SAXS) were obtained using a diffractometer (Xenocs-3D SAXS, France). CS-NPS and CS-Lys-NPs solutions were purified by centrifugation, and then the washed precipitates were scanned with 10 min of exposure time at room temperature.

The UV analyses for CS-NPs and CS-lysozyme nanoparticles were performed on a UV–visible spectrophotometer (UV-2550, Japan). Samples at 0.1 mg/mL were dissolved in an acetic acid buffer (pH 5.0) for measurement. One curve was obtained after three scans.

Circular dichroism analysis was carried out to confirm the secondary structure of lysozyme with a Multifunctional CD Spectroscope (Francois Goy, MOS-450). Samples were adjusted to a concentration of 0.1 mg/mL in an aqueous buffer (pH 5.0). One curve was obtained after three scans.

2.4. Measurement of inhibition zones, minimum inhibitory concentration (MIC) and minimum bacterial concentration (MBC)

Gram positive bacteria *B. subtilis* and gram negative bacteria *E. coli* were chosen to determine the antimicrobial actions of the

prepared nanoparticles. Every assay was performed with three replications.

The disc diffusion method was employed to determine the inhibition zone of CS-NPs and CS-Lys-NPs. First, 100 μL of suspension containing 10^7 CFU/mL *E. coli or B. subtilis* was spread on Nutrient Agar (NA). The filter papers were cut into 6-mm-diameter discs, sterilized at 121 °C for 15 min, dried in an oven at 37 °C for 1 h and then placed on the petri dish containing NA. Then, 10-μL CS-NP and CS-Lys-NP solutions (5 mg/mL, dissolved in 0.25% HAc) were added dropwise onto the disc, and 0.25% HAc was used as the control.

The turbidimetric and micro-dilution methods were applied to examine MIC and MBC of CS-NPs/CS-Lys-NPs prepared at pH 5 with 0.25 mg/mL lysozyme (Qi et al., 2004). Different concentrations of each sample solution were added to approximately 10^7 CFU/mL of *E. coli* or *B. subtilis* suspended in NB. After autoclaving at 121 °C for 15 min, a series of tubes each containing 5.0 mL of culture medium were cooled to 40–50 °C. Then, 10.0 mL of CS-NPs/CS-Lys-NPs solution (10 mg/mL) was added into the first tube; 5.0 mL of solution from the first tube was transferred to the second tube after mixing, and a similar transformation was repeated. Therefore, the concentration in each test tube is half of that in the previous one. A 50-μL aliquot of a newly prepared bacterial suspension was added into each test tube. All samples were adjusted to pH 4.5 with 0.1 M NaOH for equal comparison and incubated at 37 °C for 24 h to evaluate MIC.

A 200-μL aliquot of each strain solution from each of those tubes was inoculated on NA and examined for signs of growth. Growth of bacteria was indicated by the presence of the bacteria in the original MIC tube. The concentration in the test tubes with no growth of *E. coli* or *B. subtilis* were the MBC.

2.5. Transmission electron microscope (TEM)

The antibacterial effect of CS, CS-NPs and CS-Lys-NPs against *E. coli or B. subtilis* was observed by TEM (JEM1200EX, Japan). Materials were added to bacterial cultures grown to late exponential phase. Samples were removed by copper net accompanied by staining with uranium acetate (1%, W/V) for TEM observation.

2.6. Statistical analysis

Analysis of standard deviation (SD) was performed using SPASS 19.0 (IBM Corporation, USA). Origin 8.5 (OriginLab Corporation, USA) was applied for statistical analysis. FIT2D software (http://www.esrf.eu/computing/scientific/FIT2D) was used to analyze the data obtained from SAXS. All measurements were carried out in triplicate and results were expressed as the mean ± SD (standard deviation).

3. Results and discussion

3.1. Physicochemical characterization of CS-NPs and CS-Lys-NPs

3.1.1. Determination of particle size, PDI, zeta potential

The particle size, PDI and surface charge were determined using a nano particle size and zeta potential analyzer (Table 1). At pH 4, the Z-Average was 476.2 ± 9.55 nm and 488.8 ± 10.22 nm for CS-NPs and CS-Lys-NPs, respectively, and the polydispersity index (PDI) for CS-NPs and CS-Lys-NPs was 0.67 ± 0.10 and 0.71 ± 0.17, respectively. At pH 5, an increase in PDI was observed, while the Z-Average was slightly decreased; the corresponding values were 548.1 ± 24.87 nm and 613.5 ± 15.22 nm.

Both types of nanoparticles are positively charged either at pH 4 or 5, as the presence of protonated amino groups on the surface of particles contributes to the occurrence of positive ZP values.

3.1.2. AFM observation

AFM images of CS, CS-NPs and CS-Lys-NPs were displayed in Fig. 1. CS showed a circular form, whereas CS-NPs were small dots, and the size apparently decreased. The size of CS-Lys-NPs was larger than that of CS-NPs both at pH 4 and pH 5, which was caused by the integration of lysozyme into the CS nanoparticles. Moreover, the distribution of nanoparticles per unit volume differed. More nanoparticles were prepared at pH 5 than at pH 4, which could be because the pH can affect the protonation of CS amino groups. The nanoparticles observed in Fig. 1 were consistent with the results revealed by the nano particle size and zeta potential analyzer; the particle size and PDI of CS-NPs and CS-Lys-NPs prepared at pH 4 were smaller than the values of particles prepared at pH 5.

3.1.3. FT-IR, SAXS, CD and UV absorption analysis

The FT-IR analysis was carried out to confirm the presence of CS and lysozyme and to investigate their possible interactions. The characteristic peaks of CS displayed in Fig. 2a were assigned to polysaccharide structures. The main signals in the CS spectrum included a strong and broad band at 3381 cm^{-1} that was assigned to axial O—H and N—H stretching (Britto & Campana-Filho, 2004). A band at 2875 cm^{-1} was observed, resulting from C—H stretching bands, and the band at 1651 cm^{-1} was due to the axial C=O stretching of the acetamido groups (amide I). The angular deformation of N—H bonds of the amino groups contributed to the peak at 1597 cm^{-1}. The band at 1418 cm^{-1} was attributed to the coupling of C—N axial stretching and N—H angular deformation, and a sharp band at 1379 cm^{-1} was due to a CH_3 symmetrical deformation mode. The absorption peaks at 1154 cm^{-1} and 1079 cm^{-1} were assigned to vibrations of glycosidic bonds, C—O and C—O—C stretching, which are skeletal signals of CS, serving as vital information to determine the presence of CS, especially in low amounts (Corazzari et al., 2015). Lysozyme has been well characterized by FT-IR; lysozyme has three characteristic mid-infrared regions, including amide I (1700–1600 cm^{-1}), amide II (1600–1500 cm^{-1}) and amide III (1320–1230 cm^{-1}) (Prosapio, Reverchon, & Marco, 2016). Among these three regions, amide I was believed to have interactions with secondary structures, whereas the amide III signal was ignored because of its weakness. This revealed that the absorption at 1634 cm^{-1} can be assigned to C=O stretching vibrations of the α-helix, and N—H bending and C—N stretching vibrations contribute to the band at 1532 cm^{-1}. The broad peak at 3290 cm^{-1} arises from N—H stretching of the free amino groups, and the absorption at 2961 cm^{-1} was characteristic of C—H stretching (Koshani, Aminlari, Niakosari, Farahnaky, & Mesbahi, 2014). Characteristic peaks of CS-NPs at 3384 cm^{-1} remained with almost no obvious variation compared to CS. N—H and O—H bending peak at 3384 cm^{-1} had shifted to 3423 cm^{-1} in CS-Lys-NPs, which was a clue for lysozyme interaction with chitosan nanoparticles through its hydroxyl-group. Moreover, the peak appearing at 2925 cm^{-1} was probably due to the absorption of lysozyme, suggesting the existence of lysozyme. Additionally, the amide I peak arising from axial C=O stretching of the acetamido groups at 1634 cm^{-1} was shifted to a higher wavenumber of 1644 cm^{-1}. The amide II peak due to N—H bending and C—N stretching at 1549 cm^{-1} was shifted to a lower wavenumber of 1540 cm^{-1}. The peak at 1410 cm^{-1} attributed to the coupling of C—N axial stretching and N—H angular deformation was present in both CS-NPs and CS-Lys-NPs, suggesting that the nanoparticles had retained their structure when integrated with lysozyme. The peak at 1072 cm^{-1} was shifted to a higher wavenumber of 1089 cm^{-1}, indicating that the bonds that formed the CS backbone were strengthened by the addition of lysozyme. In brief, the spectral information from FT-IR indicated that lysozyme formed nanoparticles via the N—H to the O—H groups of chitosan.

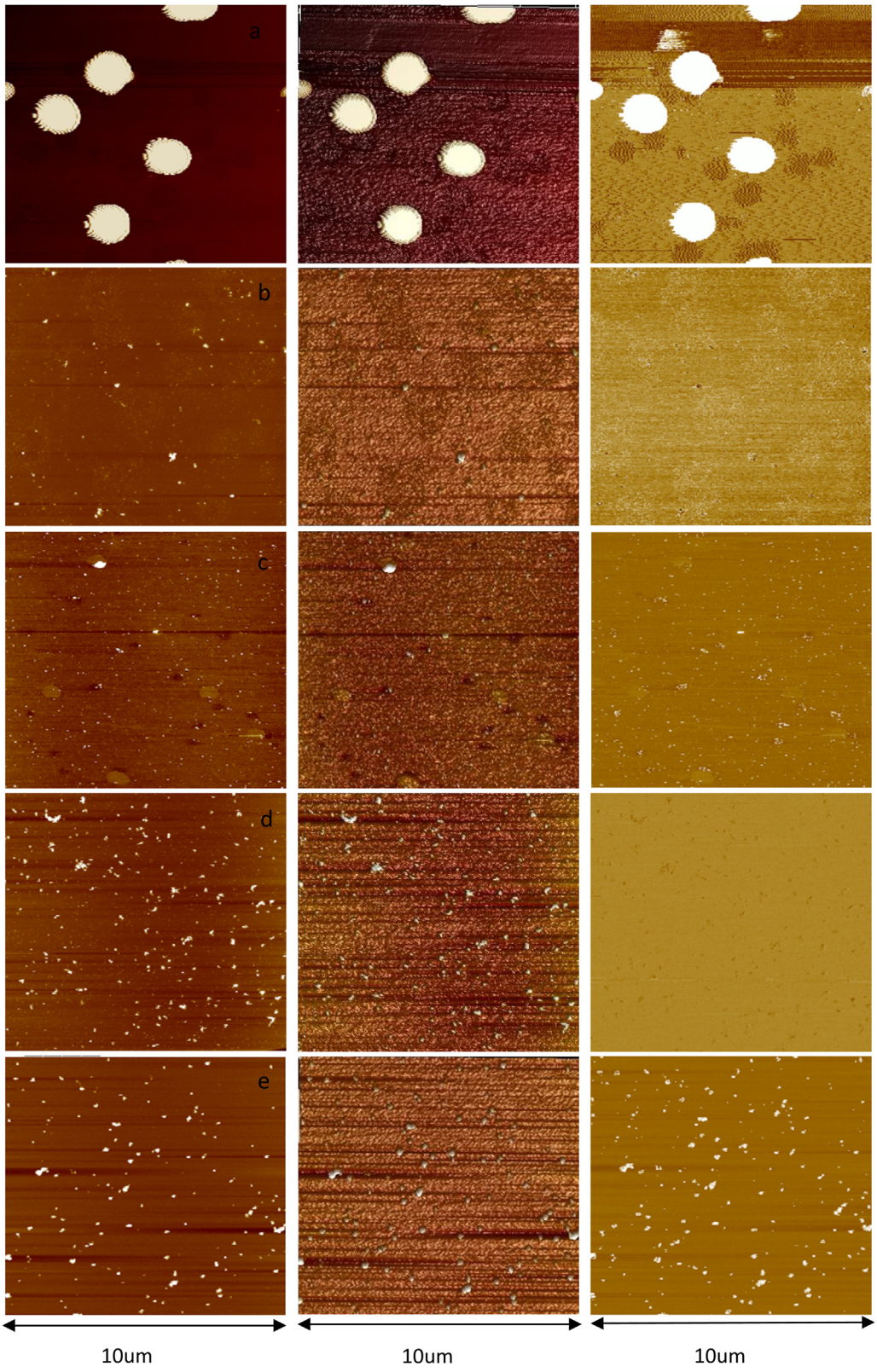

Fig. 1. Detailed AFM topographic images of CS, CS-NPs and CS-Lys-NPs.
Images (a)–(e) represent (a) CS, (b) CS-NPs prepared at pH 4, (c) CS-Lys-NPs prepared at pH 4 with a lysozyme concentration of 1.25 mg/mL, (d) CS-NPs prepared at pH 5 and (e) CS-Lys-NPs prepared at pH 5 with a lysozyme concentration of 1.25 mg/mL. From left to right: two-dimensional, three-dimensional and phase signal images.

Table 1
Particle size and zeta potential of CS-NPs and CS-Lys-NPs.

Samples	pH 4			pH 5		
	Ave-Size (nm)	PDI	ZP (mV)	Ave-Size (nm)	PDI	ZP (mV)
CS-NPs	476.2 ± 9.55	0.67 ± 0.10	17.20 ± 1.2	548.1 ± 24.87	0.92 ± 0.11	12.50 ± 0.30
CS-Lys- NPs	488.8 ± 10.22	0.71 ± 0.17	21.10 ± 0.84	613.5 ± 15.22	1.0 ± 0.14	13.6 ± 0.49

Values are given as the mean ± SD from triplicate determination. The lysozyme concentration is 1.25 mg/mL.

Small-angle X-ray scattering (SAXS) is a useful tool to explore the nanostructure of matter based on the detection of X-rays scattered by the sample at very low angles. In the present study, SAXS was used to assay the potential interactions and conformations between CS-NPs and lysozyme. The corresponding SAXS profiles are shown in Fig. 2b. Two typical SAXS peaks could be observed at a q of 0.09–0.14 nm^{-1}, indicating 45–70 nm semi-crystalline structures, while just one typical peak appeared at a q of 0.09–0.12 nm^{-1}, suggesting a 52–70 nm semi-crystalline structure according to Bragg's law $d = 2\pi/q$ (Blazek & Gilbert, 2011). Meanwhile, the increase in $I(q)$ reflected the growth of CS-Lys-NPs compared with CS-NPs (Gutsche, Guo, Dingenouts, & Nirschl, 2015), which proved the results obtained by particle size analysis and AFM observation. In addition, the peak width, which depends on the regularity of the lamellar arrangement within nanoparticles, increased with the formation of CS-Lys-NPs. This increase might be because the interaction between lysozyme and CS-NPs via N—H and O—H groups can influence the compression caused by lamellar 'buckling'. This led to a change in the distribution of lamellar sizes; thus, the SAXS peak width was slightly broadened (Yang et al., 2016).

Circular dichroism (CD) is an excellent method to detect protein conformations. Fig. 2c shows the circular dichroism spectra of lysozyme (dashed line), CS-NPs (dotted line) and CS- Lys-NPs (solid line). As shown in Fig. 2c, there was no signal for CS-NPs. The spectrum of lysozyme includes a negative band at a wavelength area shorter than 240 nm assigned to the α-helical structure containing two negative minima bands at approximately 208 (π–π* transition of the α-helix) and 222 nm (π–π* transition for both the α-helix and random coil) (Hegde, Sandhya, & Seetharamappa, 2013). As seen from Fig. 2c, a slight decrease in the ellipticity magnitude (10^{-3} deg) was observed in the characteristic spectrum of lysozyme when loaded with CS-NPs, which may be due to the interactions

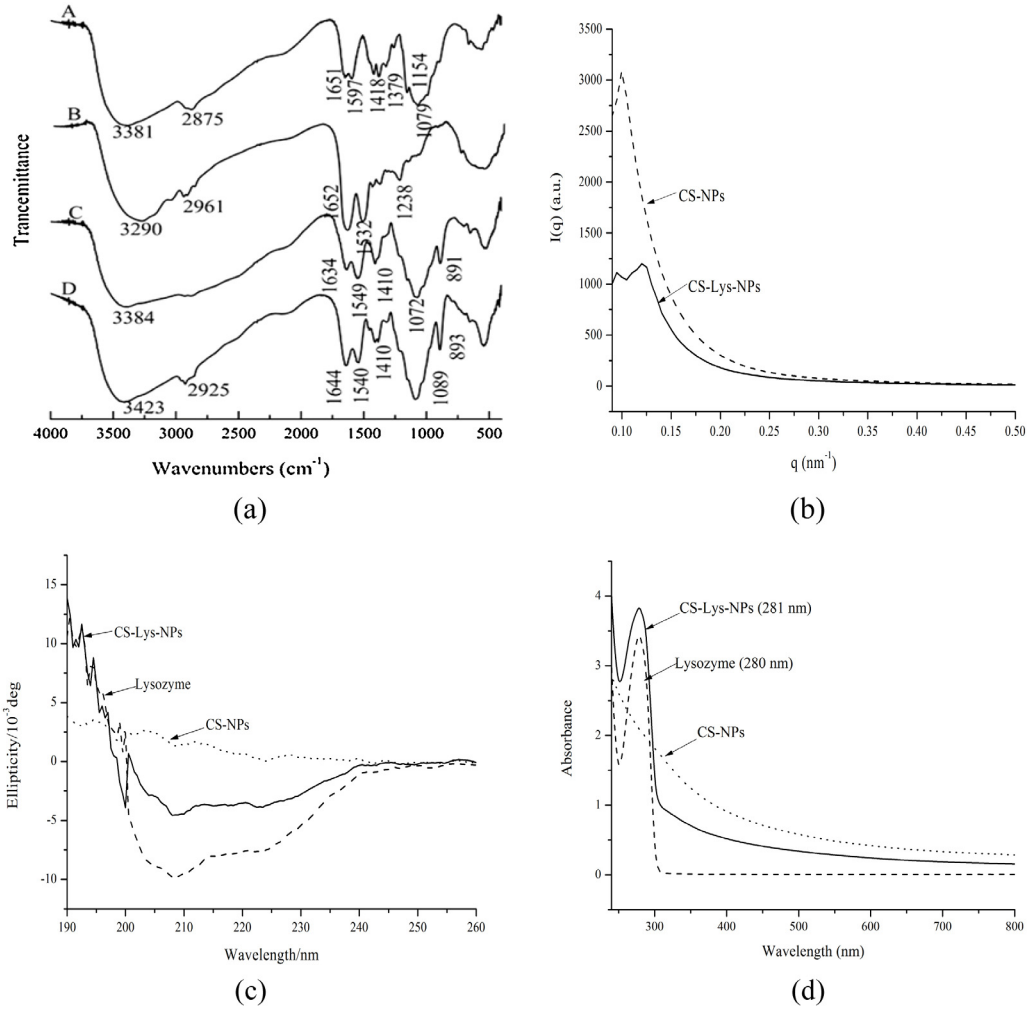

Fig. 2. (a) FTIR profiles of nanoparticles, in the figure, (A) CS, (B) lysozyme, (C) CS-NPs, (D) CS-Lys-NPs; (b) SAXS of patterns of nanoparticles; (c) circular dichroism spectra of nanoparticles; (d) UV–vis absorption spectra of nanoparticles.
In the figure, CS-NPs were prepared at pH 5 and CS-Lys-NPs were prepared at pH 5 with a lysozyme concentration of 1.25 mg/mL.

between lysozyme (N—H) and chitosan nanoparticles (O—H) proved by FT-IR. Moreover, the new band that appeared at 201 nm could be due to the newly formed hydrogen bond. In brief, the change in the CD spectrum indicated an alteration in the lysozyme conformation due to the reduction of the α-helix content (Billsten, Wahlgren, Arnebrant, Mcguire, & Elwing, 1995) and changes to the hydrogen bond environment.

To study the complex behavior between CS-NPs and lysozyme, the absorbance of lysozyme, CS-NPs and CS-Lys-NPs was examined (Fig. 2d) using UV–vis spectroscopy. CS-NPs showed no absorption peak at 280 nm; absorbance at 280 nm is characteristic of the presence of protein in a sample. Both lysozyme and CS-Lys-NPs exhibited a major band at approximately 280 nm due to the presence of a set of its constituent amino acids. In the presence of CS-NPs, the optical density increased, and a slight red shift of approximately 1 nm was observed. This could result from the formation of a ground state complex between lysozyme and CS-NPs. The increase in the absorbance demonstrates that CS-Lys-NPs has a higher extinction coefficient compared to free lysozyme. Similar studies have been conducted by Revathi, Rameshkumar, and Sivasudha (2016), who found that the absorbance increased and a slight red shift of ~5 nm occurred in lysozyme when binding of lysozyme with $AgTiO_2$ nanoparticles.

3.2. Encapsulation efficiency (%EE)

The percentage of encapsulation efficiency of CS-Lys-NPs was examined at pH 4 and pH 5 with five different concentrations of lysozyme (0.25, 0. 5, 0.75, 1.00 and 1.25 mg/mL) in the supernatant by UV–vis spectrophotometry. The% EE at pH 4 was significantly increased compared with that at pH 5 (Fig. 3a). This result verified that pH might influence the rate of lysozyme encapsulation by CS. When the concentration of lysozyme was 1.25 mg/mL at pH 4, the% EE exhibited maximum values, suggesting that more than 80% of lysozyme was efficiently loaded in CS-NPs. The%EE of CS-Lys-NPs was found to increase as the concentration of lysozyme increased from 0.25 to 1.25 mg/mL, whether at pH 4 or pH 5.

3.3. In vitro release

The addition of lysozyme at 1.25 mg/mL prepared at pH 5 was selected as the material for detecting the release rate in phosphate buffer (pH 7.4) (Fig. 3b). A 2 mg CS-Lys-NPs was dispensed into a centrifuge tube containing 4 mL of 0.02 M phosphate buffer. The suspensions were stirred and ultrasound 10 min and maintained at room temperature under shaking at 150 rpm. And then the supernatant was centrifugation at 10000*g* for 10 min. A 3 mL supernatant was withdrawn for UV–vis spectrophotometer determination. And then 3 mL of 0.02 M phosphate buffer was added into the centrifuge tube for the next measurement. The release profile of lysozyme from CS-Lys-NPs as measured by UV–vis spectrophotometry suggested that the release rate increased over time within 300 min. The maximum release was approximately 14% after 240 min, indicating that nearly 86% of lysozyme was trapped in the nanoparticles. This revealed that CS-Lys-NPs could prolong its release and remain in the matrix for a longer time, which can be a benefit to bactericidal action when used as a preservative. Similarly, the release of naringenin from CS-NPs was reported to be approximately 15% at a CS:TPP ratio of 5:1 (Kumar, Birundha, Kaveri, & Devi, 2015). Other study revealed that the release rate of BSA from CS-NPs was 20–40% (Hua, Alsarra, & Neau, 2002). And the cumulative release of Lysozyme from chitosan hydrogel composites varied from 33.32% to 65.4% (Dragan, Cocarta, & Gierszewska, 2016) under different conditions. It can be estimated that the release of lysozyme from CS-NPs could possibly be controlled under different conditions, such as integrating lysozyme into different sizes of CS-NPs or changing the pH of the release media.

3.4. Antibacterial analysis

3.4.1. Assay of inhibition zone, MIC, MBC

The antibacterial activities of CS-NPs and CS-Lys-NPs against *E. coli* and *B. subtilis* were investigated, and the results are presented in Table 2. According to the results of the disc diffusion method, the inhibition zone diameters of the CS-NPs and CS-Lys-NPs were 10.34 ± 1.21 and 13.11 ± 0.48 mm for *E.coli*, 11.70 ± 1.51 and 12.89 ± 1.25 mm for *B.subtilis*, respectively. Additionally, the inhibition zone diameters of CS-Lys-NPs significantly increased to 126.79% for *E.coli*, and 110.17% for *B.subtilis* of the initial level in the presence of CS-NPs. Therefore, CS-Lys-NPs had higher antimicrobial activities against both *E. coli and B. subtilis* than CS-NPs based on inhibition zone diameters.

The sensitivities of *E. coli* and *B. subtilis* to CS-NPs and CS-Lys-NPs were also determined by the minimal inhibitory concentration (MIC) values. The MIC values of CS-NPs were 5/8 mg/mL, but the CS-Lys-NP concentration of 5/32 mg/mL was sufficient to elicit complete inactivation of *E. coli*, and the corresponding values for *B. subtilis* were 5/16, 5/32 mg/mL, respectively, indicating the enhanced sensitivity of *E. coli and B. subtilis* when lysozyme was integrated into CS-NPs. These values were much lower than the MIC value of 0.1 mg/mL used to examine antimicrobial effects of CS for *E. coli* in a previous study (Croisier & Jérôme, 2013; Younes, Sellimi, Rinaudo, Jellouli, & Nasri, 2014).

As shown in Table 2, for CS-NPs, concentrations of 5/2, 5/4 mg/mL were required to elicit complete inactivation of *E. coli* and *B. subtilis*, respectively, while that value decreased to 5/16 mg/mL for CS-Lys-NPs to eliminate these two bacteria. The significant difference between the values of MBC for CS-NPs and CS-Lys-NPs may contribute to the changes in cell morphology (Fig. 4) when the concentration was 1 mg/mL for both nanoparticles.

3.4.2. Antimicrobial mechanism

To better understand the interactions between CS-NPs/CS-Lys-NPs and *E.coli/B. subtilis*, TEM was carried out to investigate the changes in cell morphology before and after exposure to 1 mg/mL CS/CS-NPs/CS-Lys-NPs. As shown in Fig. 4a_1-d_1, comparison of *E.coli* before exposure to nanoparticles, which exhibited a round columna, a slight change in the membrane but retention of its general shape was observed upon treatment with 1 mg/mL CS. When treated with 1 mg/mL CS-NPs, there was breakage of the basement membrane and leakage of some cytoplasm. Conversely, the cells were degraded from a round columna to an irregular shape, and complete rupture was observed when treated with 1 mg/mL CS-Lys-NPs. This revealed that the effect of CS-Lys-NPs against *E. coli* was superior to that of CS-NPs, while CS exhibited the worst antibacterial effect on *E. coli*. The improved ability of CS-Lys-NPs to enter into the cell and interfere with protein synthesis resulted in the death of *E. coli* (Nakayama et al., 2012). Moreover, CS-Lys-NPs had higher PDIs and zeta potentials than CS-NPs, which was detrimental to the growth of *E. coli*, damaging the cell membrane and leading to leakage of the granulated content of the inner cell (Zhang, Jung, & Zhao, 2016).

As shown in Fig. 4a_2-d_2, the size of *B. subtilis* decreased no matter treated by CS, CS-NPs, or CS-Lys-NPs with respect to the control group. Comparison of *B. subtilis* before exposure to nanoparticles, which was cylindrical in shape with large numbers of flagella, a significant change in the integrity of flagella but retention of its general shape was observed upon treatment with 1 mg/mL CS. Additionly, the flagella were completely destroyed by the treatment of 1 mg/mL CS-NPs or CS-Lys-NPs. Wherein, *B. subtilis* maintained its general morphology in the CS-NPs group, while cells proliferation was

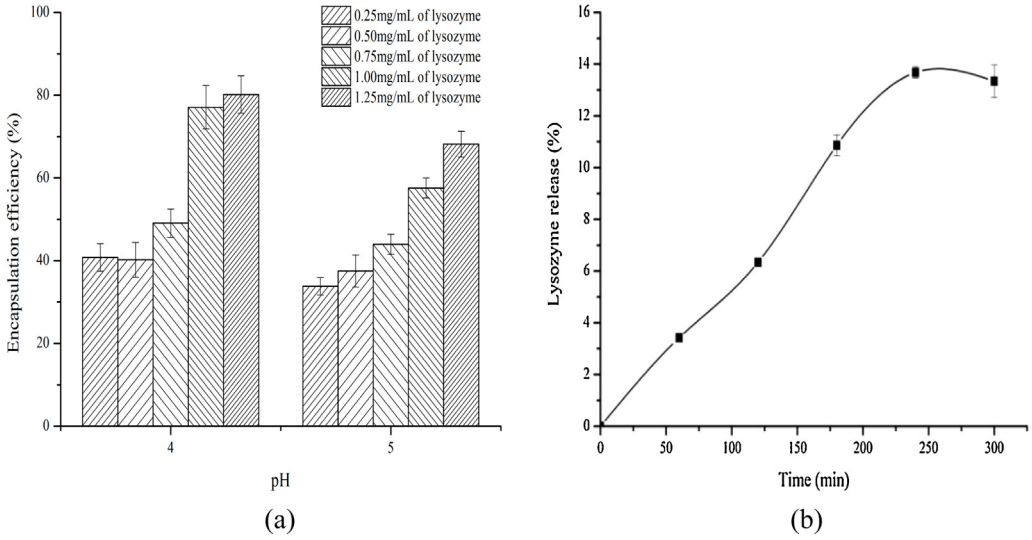

Fig. 3. (a) Efficiency of encapsulation of lysozyme by CS in pH 4 and 5. Five different concentrations of lysozyme of 0.25, 0. 50, 0.75, 1.00 and 1.25 mg/mL were used; (b) The release spectrophotometer of lysozyme from CS-Lys-NPs. CS-Lys-NPs was prepared in pH 5 with lysozyme concentrations of 1.25 mg/mL.

Table 2
Inhibition results of nanoparticles.

Treatment group	*E. coli*			*B. Subtilis*		
	Inhibition zone (mm)	MIC (mg/mL)	MBC (mg/mL)	Inhibition zone (mm)	MIC (mg/mL)	MBC (mg/mL)
CS	R	ND	ND	R	ND	ND
CS-NPs	10.34 ± 1.21	5/8	5/2	11.70 ± 1.51	5/16	5/4
CS-Lys- NPs	13.11 ± 0.48	5/32	5/16	12.89 ± 1.25	5/32	5/16

Values are given as the mean ± SD from triplicate determination. The zone (mm), MIC (mg/mL) and MBC (mg/mL) of CS-NPs (prepared at pH 5), CS-Lys-NPs (prepared at pH 5 with lysozyme concentration of 1.25 mg/mL) suspension against *E. coli*/*B. subtilis* in 0.25% HAc. CS, CS-NPs and CS-Lys-NPs are at a concentration of 5 mg/mL. R: resistant; ND: No determined. Acetic acid (0.25%) was used as a negative control.

inhibited with ill-defined contours when treated by 1 mg/mL CS-Lys-NPs. This was consistent with the result in the published work (Katas & Alpar, 2006), where better activity of nanoparticles is presented due to their nano size and larger surface area available for the interactions with microbial cell wall. Generally, flagella are organs of locomotion for bacteria, which make contact and surround the cells. They can remain stuck by the polymeric substances produced by bacteria and fixed in a position around the cell border which may favour bacterial movement to abandon the trench and join the neighbouring microbes (Díaz, Schilardi, Salvarezza, & Mele, 2011). The flagellum is vital for active movement of flagellated bacteria in an aqueous environment and for chemotaxis

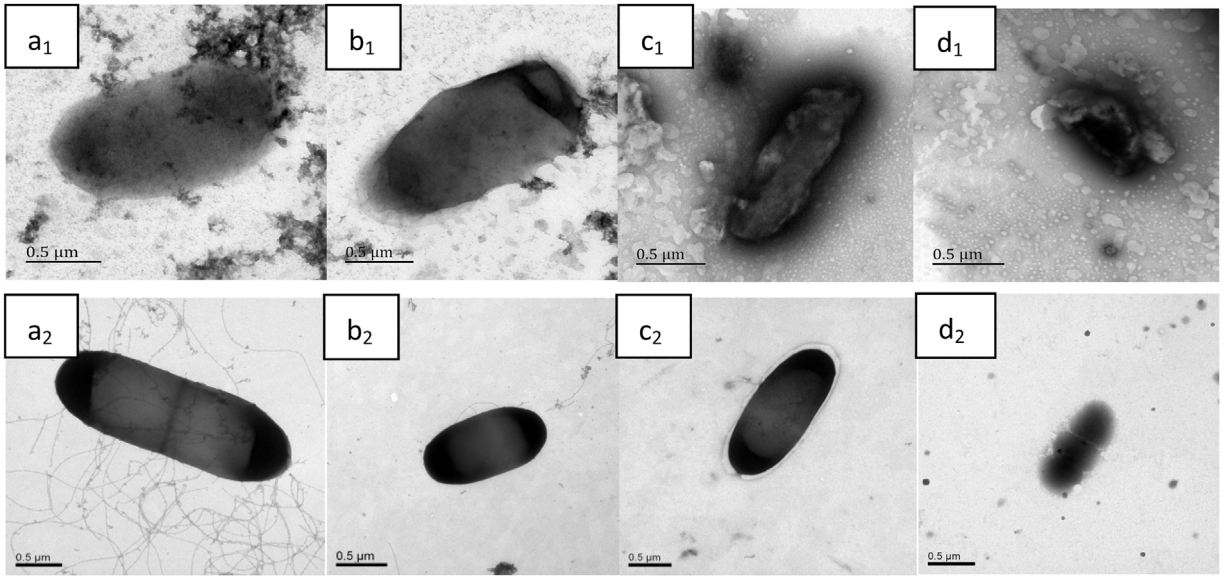

Fig. 4. TEM micrographs of *E.coli* (a_1, b_1, c_1, d_1) and *B.subtilis* (a_2, b_2, c_2, d_2) treated by nanoparticles.
($a_{1,2}$) The control; ($b_{1,2}$) treated by 1 mg/mL CS; ($c_{1,2}$) treated by 1 mg/mL CS-NPs; ($d_{1,2}$) treated by 1 mg/mL CS-Lys-NPs.

and significantly affects the interaction with surfaces (Senesi et al., 2004). The major chemical component of flagella is protein and their assembly requires ordered export of thousands of structural subunits across the cell membrane (Evans, Hughes, & Fraser, 2014). The positively charged CS, CS-NPs or CS-Lys-NPs can influence metabolism enzyme activities, which have adverse impact on the synthesis of esstial elements (e.g. amino acid, polypeptide) and interfere with bacterial metabolism. The destruction of flagella could have different explanations, such as lower transcription rate, decreased stability of the protein, or slower assembly of the flagellin monomers caused by CS, CS-NPs or CS-Lys-NPs. Interstingly, apart from the disappearing of flagellum in the CS-Lys-NPs group, the outline of *B. subtilis* was blurry, and the gap junction inside the cells was observed, indicating the damage of membrane, formation of tissue space. This may be due to the higher PDIs and zeta potentials of CS-Lys-NPs, which have a larger momentum to penetrate into the cell membrane barrier.

Currently, the exact mechanisms of the antimicrobial activity of CS, CS-NPs and their derivatives are not absolutely understood. However, two major mechanisms for the antimicrobial action of CS have been postulated: (1) Stacking at the cell surface of bacteria, positively charged CS can interfere with bacterial metabolism; (2) CS can penetrate through the cell membrane and then adsorb onto DNA molecules, blocking the transcription of RNA from DNA. For this mechanism, the antimicrobial activities of CS have a strong association with its physical characteristics, such as molecular weight and degree of deacetylation (Benhabiles et al., 2012). The molecular weight of CS should be less than ~5000 Da to be able to permeate into cells (Liu, Yun, Dong, Zhi, & Kang, 2001).

Lysozyme has been shown to have anti-bacterial effects in vivo studies. Early in 1992, Fleming found that lysozyme can inhibit some Gram-positive bacteria by hydrolyzing the cell walls (Jollès, 1964). Lysozyme immobilized on chitosan beads was reported to have antimicrobial activity in wine (Liburdi et al., 2015). Lysozyme incorporated into nano-fibrous mats was effective against *E. coli* and *S. aureus* (Wei et al., 2014). Owing to the biological activities, lysozyme and its complex played important roles in food packaging, food preservatives and wound dressing. The mode of its antimicrobial action depended upon the hydrolysis of 1,4-β-linkage between *N*-acetyl-muramic acid and *N*-acetyl-D-glucosamine residues in a peptidoglycan and between *N*-acetyl-D-glucosamine residues in chitodextrin catalyzed by lysozyme, damaging bacterial cell walls (Yuan et al., 2013).

Integration of lysozyme into CS-NPs exhibited higher antibacterial activity than CS-NPs and remarkably higher antibacterial activity than CS itself. Due to the interaction between lysozyme and CS-NPs via the N—H and O—H groups and the absorption of lysozyme into CS-NPs, the average zeta potential of CS-Lys-NPs increased. Meanwhile, a larger number of positive charges can strongly affect the antimicrobial activity of CS and its derivatives (Rabea, Badawy, Stevens, Smagghe, & Steurbaut, 2003). Thus, the higher surface charge density of CS-Lys-NPs may be responsible for its higher antibacterial activity against *E. coli* and *B. subtilis* because of the improved affinity with the bacterial membrane and increased interference with the bacterial metabolism.

4. Conclusions

CS-NPs prepared based on the method of ionotropic gelation between CS and sodium tripolyphosphate (TPP) was reported in the literature. In the present study, CS-NPs were prepared, and lysozyme was integrated into CS-NPs via ionotropic gelation technology by the interaction between N—H and O—H groups. The nanoparticles were positively charged and small in size, which could enhance the antimicrobial activities against bacteria. This study showed that CS-NPs and CS-Lys-NPs can markedly inhibit the growth of *E. coli* and *B. subtilis,* and they exhibited higher antibacterial activity than CS. Additionally, among the nanoparticles, CS-Lys-NPs proved to be the best choice for *E. coli* and *B. subtilis* growth inhibition based on inhibition zone, MIC and MBC. TEM micrographs of gram negtive bacteria *E. coli* revealed that the antibacterial action was probably due to the ability of CS-NPs/CS-Lys-NPs to penetrate the cell membrane, which caused leakage of the cytoplasm and eventual cell death. Besides, the antibacterial activity agagnist gram positive bacteria *B. subtilis* may be attributed to CS-NPs/CS-Lys-NPs can influence metabolism enzyme activities and interfere with bacterial metabolism. Consequently, with higher PDIs and zeta potentials, CS-Lys-NPs was more effective in inhibiting *E. coli* or *B. subtilis* compared to CS-NPs. It is anticipated that CS-Lys-NPs could be applied broadly in the food industry and could have other applications in the form of direct addition or incorporation into packaging.

Acknowledgement

This work was financed by National Key Research and Development Program (2016YFD0400102).

Appendix A. Supplementary data

Supplementary data associated with this article can be found, in the online version, at http://dx.doi.org/10.1016/j.carbpol.2016.08.076.

References

Amara, C. B., Eghbal, N., Degraeve, P., & Gharsallaoui, A. (2016). Using complex coacervation for lysozyme encapsulation by spray-drying. *Journal of Food Engineering*, *183*, 50–57.

Benhabiles, M. S., Salah, R., Lounici, H., Drouiche, N., Goosen, M. F. A., & Mameri, N. (2012). Antibacterial activity of chitin, chitosan and its oligomers prepared from shrimp shell waste. *Food Hydrocolloids*, *29*, 48–56.

Billsten, P., Wahlgren, M., Arnebrant, T., Mcguire, J., & Elwing, H. (1995). Structural changes of t4 lysozyme upon adsorption to silica nanoparticles measured by circular dichroism. *Journal of Colloid & Interface Science*, *175*, 77–82.

Blazek, J., & Gilbert, E. P. (2011). Application of small-angle x-ray and neutron scattering techniques to the characterisation of starch structure: A review. *Carbohydrate Polymers*, *85*, 281–293.

Britto, D. D., & Campana-Filho, S. P. (2004). A kinetic study on the thermal degradation of N,N,N–trimethylchitosan. *Polymer Degradation & Stability*, *84*, 353–361.

Chen, X., Niyonsaba, F. H., Okuda, D., Nagaoka, I., Ikeda, S., Okumura, K., et al. (2005). Synergistic effect of antibacterial agents human beta-defensins, cathelicidin ll-37 and lysozyme against Staphylococcus aureus and Escherichia coli. *Journal of Dermatological Science*, *40*, 123–132.

Corazzari, I., Nistico, R., Turci, F., Faga, M. G., Franzoso, F., Tabasso, S., et al. (2015). Advanced physico-chemical characterization of chitosan by means of TGA coupled on-line with FTIR and GCMS: Thermal degradation and water adsorption capacity. *Polymer Degradation and Stability*, *112*, 1–9.

Croisier, F., & Jérôme, C. (2013). Chitosan-based biomaterials for tissue engineering. *European Polymer Journal*, *49*, 780–792.

Díaz, C., Schilardi, P. L., Salvarezza, R. C., & Mele, M. F. L. D. (2011). Have flagella a preferred orientation during early stages of biofilm formation? AFM study using patterned substrates. *Colloids & Surfaces B Biointerfaces*, *82*, 536–542.

Dekina, S., Romanovska, I., Ovsepyan, A., Tkach, V., & Muratov, E. (2016). Gelatin/carboxymethyl cellulose mucoadhesive films with lysozyme: Development and characterization. *Carbohydrate Polymers*, *147*, 208–215.

Dragan, E. S., Cocarta, A. I., & Gierszewska, M. (2016). Designing novel macroporous composite hydrogels based on methacrylic acid copolymers and chitosan and in vitro assessment of lysozyme controlled delivery. *Colloids & Surfaces B Biointerfaces*, *139*, 33–41.

Evans, L. D. B., Hughes, C., & Fraser, G. M. (2014). Building a flagellum outside the bacterial cell. *Trends in Microbiology*, *22*, 566–572.

Foged, C., Brodin, B., Frokjaer, S., & Sundblad, A. (2015). Particle size and surface charge affect particle uptake by human dendritic cells in an in vitro model. *International Journal of Pharmaceutics*, *298*, 315–322.

Gutsche, A., Guo, X., Dingenouts, N., & Nirschl, H. (2015). Synthesis and small angle x-ray scattering (saxs) characterization of silica spheres covered with gel-like particles formed by means of solvent evaporation. *Powder Technology*, *278*, 257–265.

Hegde, A. H., Sandhya, B., & Seetharamappa, J. (2013). Investigations to reveal the nature of interactions of human hemoglobin with curcumin using optical techniques. *International Journal of Biological Macromolecules*, *52*, e26686.
Hong, K. N., Na, Y. P., Lee, S. H., & Meyers, S. P. (2002). Antibacterial activity of chitosans and chitosan oligomers with different molecular weights. *International Journal of Food Microbiology*, *74*, 65–72.
Hua, Z., Alsarra, I. A., & Neau, S. H. (2002). An in vitro evaluation of a chitosan-containing multiparticulate system for macromolecule delivery to the colon. *International Journal of Pharmaceutics*, *239*, 197–205.
Jang, K. I., & Lee, H. G. (2008). Stability of chitosan nanoparticles for l –ascorbic acid during heat treatment in aqueous solution. *Journal of Agriculture and Food Chemistry*, *56*, 1936–1941.
Jash, C., & Kumar, G. S. (2014). Binding of alkaloids berberine, palmatine and coralyne to lysozyme: A combined structural and thermodynamic study. *RSC Advances*, *4*, 12514–12525.
Jing, J., Chang, Z., Zeng, G. M., Gong, J. L., Chang, Y. N., Song, B., et al. (2016). The disinfection performance and mechanisms of Ag/lysozyme nanoparticles supported with montmorillonite clay. *Journal of Hazardous Materials*, *317*, 416–429.
Jing, M., Song, W., & Liu, R. (2016). Binding of copper to lysozyme: Spectroscopic, isothermal titration calorimetry and molecular docking studies. *Spectrochimica Acta Part A Molecular & Biomolecular Spectroscopy*, *164*, 103–109.
Jollès, P. (1964). Recent developments in the study of lysozymes. *Angewandte Chemie International Edition in English*, *3*, 28–36.
Katas, H., & Alpar, H. O. (2006). Development and characterisation of chitosan nanoparticles for siRNA delivery. *Journal of Controlled Release*, *115*, 216–225.
Koshani, R., Aminlari, M., Niakosari, M., Farahnaky, A., & Mesbahi, G. (2014). Production and properties of tragacanthin-conjugated lysozyme as a new multifunctional biopolymer. *Food Hydrocolloids*, *47*, 69–78.
Kumar, S. P., Birundha, K., Kaveri, K., & Devi, K. T. R. (2015). Antioxidant studies of chitosan nanoparticles containing naringenin and their cytotoxicity effects in lung cancer cells. *International Journal of Biological Macromolecules*, *78*, 87–95.
Liao, Y. H., Brown, M. B., Nazir, T., Quader, A., & Martin, G. P. (2002). Effects of sucrose and trehalose on the preservation of the native structure of spray-dried lysozyme. *Pharmaceutical Research*, *19*, 1847–1853.
Liburdi, K., Benucci, I., Palumbo, F., & Esti, M. (2015). Lysozyme immobilized on chitosan beads: Kinetic characterization and antimicrobial activity in white wines. *Food Control*, *63*, 46–52.
Liu, X., Yun, L., Dong, Z., Zhi, L., & Kang, D. (2001). Antibacterial action of chitosan and carboxymethylated chitosan. *Journal of Applied Polymers Science*, *79*, 1324–1335.
Nakayama, M., Shigemune, N., Tsugukuni, T., Jun, H., Matsushita, T., Mekada, Y., et al. (2012). Mechanism of the combined antibacterial effect of green tea extract and NaCl against Staphylococcus aureus and Escherichia coli O_{157}:H_7. *Food Control*, *25*, 225–232.
Prosapio, V., Reverchon, E., & Marco, L. D. (2016). Production of lysozyme microparticles to be used in functional foods, using an expanded liquid antisolvent process. *Journal of Supercritical Fluids*, *107*, 106–113.
Qi, L., Xu, Z., Jiang, X., Hu, C., & Zou, X. (2004). Preparation and antibacterial activity of chitosan nanoparticles. *Carbohydrate Research*, *339*, 2693–2700.
Rabea, E. I., Badawy, M. E., Stevens, C. V., Smagghe, G., & Steurbaut, W. (2003). Chitosan as antimicrobial agent: Applications and mode of action. *Biomacromolecules*, *4*, 1457–1465.
Ravindra, R., Krovvidi, K. R., & Khan, A. A. (1998). Solubility parameter of chitin and chitosan. *Carbohydrate Polymers*, *36*, 121–127.
Revathi, R., Rameshkumar, A., & Sivasudha, T. (2016). Spectroscopic investigations on the interactions of $AgTio_2$ nanoparticles with lysozyme and its influence on the binding of lysozyme with drug molecule. *Spectrochimica Acta Part A Molecular Spectroscopy*, *152*, 192–198.
Sanyakamdhorn, S., Agudelo, D., & Tajmir-Riahi, H. A. (2013). Encapsulation of antitumor drug doxorubicin and its analogue by chitosan nanoparticles. *Biomacromolecules*, *14*, 557–563.
Senesi, S., Ghelardi, E., Celandroni, F., Salvetti, S., Parisio, E., & Galizzi, A. (2004). Surface-associated flagellum formation and swarming differentiation in Bacillus subtilis are controlled by the ifm locus. *Journal of Bacteriology*, *186*, 1158–1164.
Tiwari, B. K., Valdramidis, V. P., O'Donnell, C. P., Muthukumarappan, K., Bourke, P., & Cullen, P. J. (2009). Application of natural antimicrobials for food preservation. *Journal of Agricultural & Food Chemistry*, *57*, 5987–6000.
Wei, L., Li, X., Wang, Q., Pan, Y., Wang, T., Wang, H., et al. (2014). Antibacterial activity of nanofibrous mats coated with lysozyme-layered silicate composites via electrospraying. *Carbohydrate Polymers*, *99*, 218–225.
Yang, Z., Gu, Q., Lam, E., Tian, F., Chaieb, S., & Hemar, Y. (2016). In situ study starch gelatinization under ultra-high hydrostatic pressure using synchrotron SAXS. *Food Hydrocolloids*, *56*, 58–61.
Yong, L., Yan, S., Xu, Y., Hai, F., Fu, S., Tang, J., et al. (2013). Preparation and evaluation of lysozyme-loaded nanoparticles coated with poly-γ-glutamic acid and chitosan. *International Journal of Biological Macromolecules*, *59*, 201–207.
Younes, I., Sellimi, S., Rinaudo, M., Jellouli, K., & Nasri, M. (2014). Influence of acetylation degree and molecular weight of homogeneous chitosans on antibacterial and antifungal activities. *International Journal of Food Microbiology*, *185*, 57–63.
Yuan, S., Yin, J., Jiang, W., & Liang, B. (2013). Enhancing antibacterial activity of surface-grafted chitosan with immobilized lysozyme on bioinspired stainless steel substrates. *Colloids & Surfaces B Biointerfaces*, *106C*, 11–21.
Zhang, T., Zhou, P., Zhan, Y., Shi, X., Lin, J., Du, Y., et al. (2015). Pectin/lysozyme bilayers layer-by-layer deposited cellulose nanofibrous mats for antibacterial application. *Carbohydrate Polymers*, *117*, 687–693.
Zhang, H., Jung, J., & Zhao, Y. (2016). Preparation, characterization and evaluation of antibacterial activity of catechins and catechins–Zn complex loaded β-chitosan nanoparticles of different particle sizes. *Carbohydrate Polymers*, *137*, 82–91.
Zheng, L., Wan, Y., Yu, L., & Zhang, D. (2016). Lysozyme as a recognition element for monitoring of bacterial population. *Talanta*, *146*